The use of an unmanned aerial vehicle to acquire data to develop inland electronic navigational charts: The case of a bridge and the navigation infrastructure located on it

Jacek Łubczonek

https://orcid.org/0000-0002-9400-3426

Maritime University of Szczecin, Chair of Geoinformatics
46 Żołnierska St., 71-210 Szczecin, Poland
e-mail: j.lubczonek@am.szczecin.pl

Abstract
Unmanned aerial vehicle (UAV) technologies are becoming increasingly common, with ever-expanding applications. Low-altitude imaging makes it possible to quickly acquire high-resolution data for various objects, especially for mapping. This paper presents the mapping of a bridge and its notice marks, lights, and span to produce electronic navigation charts for inland navigation. The research object was the Clowy Bridge on the Regalica River in Szczecin, Poland. In order to carry out the research, two photogrammetric flights were made, and three sets of photos were created, from which orthophotos were developed. The research included the analysis of the orthophoto generation process, as well as quantitative and qualitative analyses. The results of the research demonstrated the possibility of using this type of data for mapping bridges to create electronic navigation maps for inland navigation.

Introduction

One of the basic navigation aids is electronic charts, which cover inland waterways and should ensure the safe navigation of a ship. In navigational charts, a special group are objects that restrict navigation. Such objects undoubtedly include bridges, which often limit the transit capacity of ships by narrowing the waterways within the limits of the navigable span and the vertical clearance (Kujawski, Jerzyło & Rekowska, 2018). For this reason, bridges are often collision structures (Knott & Winters, 2018), which unfortunately can lead to the temporary exclusion of the navigable route and road infrastructure or the loss of many lives; therefore, navigation near bridges should be adequately supported by various navigational aids (Chen & Duan, 2003), such

as notice marks, lights, and radar reflectors. These aids are used in terrestrial navigation and are also mapped in navigation charts. Given their particular importance, it is essential to ensure that such data are mapped with sufficient accuracy and timeliness.

Nowadays, it is common to use imaging materials acquired using photogrammetric platforms to create maps. Until recently, the only source of high-resolution data was aerial orthophoto maps; however, their resolution and processing make it impossible to map objects such as bridges due to radial distortions of land objects. An alternative to aerial photogrammetry is low-altitude photogrammetry, which in recent years has provided new opportunities for spatial data acquisition. The unquestionable advantages of this technology include the relatively low costs of data acquisition, the acquisition of spatial data of various

topographic and engineering objects, measurements in places that are difficult to access, or the creation of photogrammetric products with very high resolution. This technology has a very wide application range, including map creation and updating (Koeva et al., 2018), coastal bathymetry mapping (Tsukada, Shimozono & Matsuba, 2020), biomass mapping (Lopatin & Lopatina, 2017), topographic surface elevation change mapping (Lizarazo, Angulo Morales & Rodríguez Galvis, 2017), shoreline mapping (Łubczonek, Łącka & Zaniewicz, 2019), analysis of coastal zones (Lowe et al., 2019, Angnuureng et al., 2020, Burdziakowski et al., 2020, Casella et al., 2020, Contreras-de-Villar at al., 2021), and many others.

Unmanned aerial vehicle (UAV) technology is also used for bridge inspections, whose advantages include a faster inspection time, better access to the bridge, and to reduce overall process costs. Any inspection should also take into account the design of the UAV, including the cameras, data acquisition method, and geometric resolution (Khaloo et al., 2018). Interesting solutions include drone contact measurements of bridge structures (Ikeda et al., 2018), imaging of concrete delamination using video and infrared cameras (Escobar-Wolf et al., 2018), the use of passive infrared sensors for delamination detection (Mac et al., 2019), planning autonomous missions for data acquisition (Jung et al., 2019), or crack identification (Kim et al., 2018). Other interesting studies that may be useful for any work requiring image quality assessments can be found in refs. (Kedzierski et al., 2019, Burdziakowski, 2021).

This study focuses on the use of UAV technology to map bridges and the navigational infrastructure located on them to develop navigational charts. The research included both qualitative and quantitative assessments of the bridge span, notice marks, and lights (features included in standards for the production of inland electronic charts). The rationale for undertaking the research was a previous study, which used a ground-based laser scanner that unfortunately had limited capabilities for scanning lights and marks. The identified problem was the inaccurate measurement of marks due to the material used in their construction, which enhanced the reflection of light. A second problem was the poor reflection of the laser beam from the black housings of the lights (Łubczonek, 2017). A practical aspect is the possibility to acquire data of bridges where access and measurement are usually difficult (e.g., railway bridges and designated measurement times due to railway traffic) and the often limited possibility to obtain

measurements with a GPS receiver. The second case concerns the high-steel structures present on some bridges, which obscure the horizon of GPS antennae, making an accurate measurement impossible or, in some cases, preventing a measurement entirely. The advantage of UAV imaging is that a complete set of data (image information and object coordinates) can be acquired without interfering with the operation of the bridge. Such data can also be used for navigational infrastructure inventories.

Materials and methods

The research used data acquired during two photogrammetric missions with a DJI Phantom 4 Pro drone. The flights were carried out over the Clowy Bridge in the city of Szczecin, Poland. The data were processed in Pix4D software. For quantitative evaluation, the position of objects such as the outer edge of the bridge span, notice marks, and navigation light housings were measured with an RTK geodetic receiver. Table 1 summarises the basic parameters of the measuring instruments used in the study.

Table 1. Basic parameters of the measuring instruments used

DJI Phantom 4 Pro
Satellite Positioning Systems: GPS/GLONASS
Sensor: 1" CMOS, effective pixels: 20 M
Photo: JPEG, DNG (RAW), JPEG + DNG
Max Flight Time: Approx. 30 minutes
Range: 350 m
Sokkia GRX1
Number of channels: 72
Signals to be tracked: GPS, GLONASS, SBAS
Measuring frequency up to 20 Hz
RTK accuracy: H-10 mm +1 ppm, V-20 mm +1 mm

The study area included a section of land with the Clowy Bridge. The bridge is located in Poland, in the city of Szczecin, on the Regalica River (Figure 1). The Clowy Bridge is constructed of two 100 m long steel segments supported on two pillars. The materials are reinforced concrete and steel. The roadway across the bridge is covered with asphalt, while the pedestrian lane is made of a hardened layer. This lane is separated from the road by a metal safety barrier. There are railings on the outer parts of the span. The view of the bridge is shown in Figure 1.

Figure 2a, 2b, and 2c show the objects under investigation. Notice marks and navigation lights are attached to the bridge with brackets. In the case of the marks, the measurements were carried out

Figure 1. Location map of the bridge and view of the bridge and its elements: road safety barriers, railings, asphalt road, and pedestrian lane
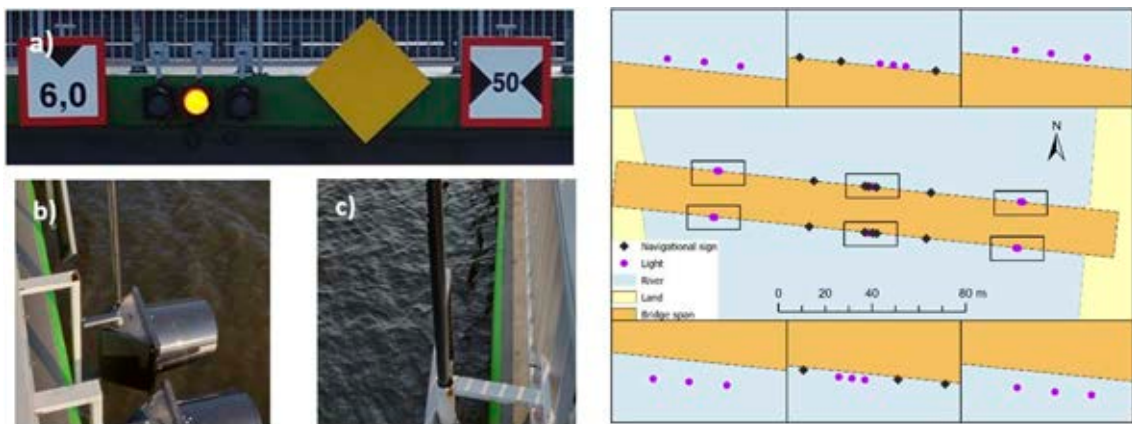

Figure 2. Objects used in the survey: a) Notice marks, navigation lights, and the side of the span (painted green), b) pole measurement of the lights, c) pole measurement of the notice marks. On the map: arrangement of lights, marks, and reflectors on the Clowy Bridge
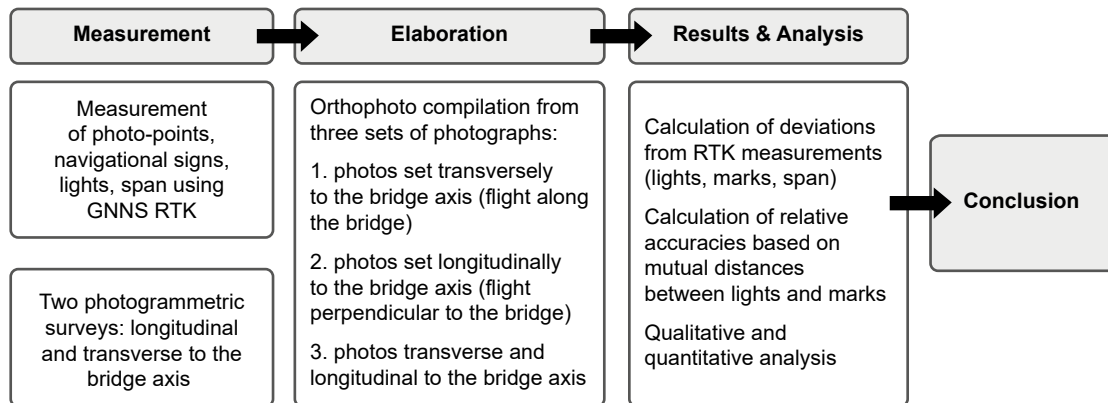

Figure 3. The research workflow

by inserting a pole through the holes in the bracket, while in the case of the lights, a pole was applied to the outer bolt. The span was measured by applying the pole to its outer edges. The location of the analyzed objects on the bridge span is illustrated in Figure 2.

The research workflow (Figure 3) consisted of the successive steps of measurement, elaboration, results & analysis, and conclusions.

Data acquisition

Images were acquired in two aerial missions, which differed in the way the bridge was framed. In the first mission, the flight was conducted along the length of the bridge. In this case, the longer side of the camera transducer was perpendicular to its axis. In the second case, the flight was carried out on courses perpendicular to the axis of the bridge, so the longer side of the transducer was parallel to the
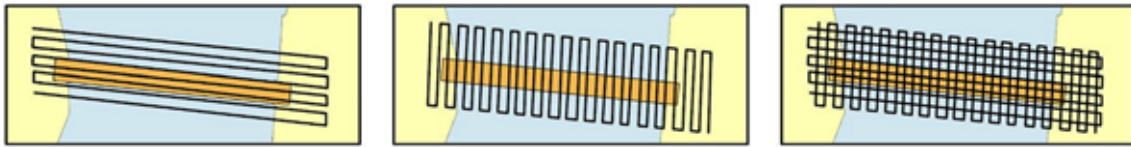
Figure 4. The flight plans for the creation of the three image data sets

axis of the bridge. This allowed for the preparation of three sets of photographs for the study: with the frame arranged transverse to the axis of the bridge, with the frame arranged perpendicular to the axis of the bridge, and a combination of the first two sets. In order to align the block of photos, a photogrammetric network was established, consisting of seven ground control points, which were located on both sides of the bridge and opposite banks. Considering the surroundings of the bridges, the possibility of establishing a photogrammetric network is usually limited due to the amount of exposed terrain. Duplication of these points in three locations was performed to prevent their possible obscuring by cars or people staying near the bridge (anglers). The coordinates of the ground control points were measured with an RTK receiver using GPS and GLONASS surface corrections of the TPI network. The average m_p measurement error was 0.007 m (based on the report generated from the GNNS/RTK measurement file). The flights were carried out at an altitude of 55 m using the DJI GS Pro application. The front and side overlap of the images was 90%. The camera settings were: aperture unit f/2.8, exposure time 1/1000 s, sensor sensitivity ISO 100, and focal length 9 mm. The flight plans for creating the three image data sets are illustrated in Figure 4.

Data processing analysis

The UAV data were processed in Pix4D software. The software allows the input of ground control point coordinates, which enable the alignment of a block of images with simultaneous registration to a coordinate system. The data processing was automated, with a choice of parameters in the following three data processing stages: "*Initial Processing*", "*Point Cloud and Mesh*", and "*DSM, Orthomosaic and Index*". For the extraction of tie points, full-scale images were selected to ensure accurate results. Optimization of image merging was carried out in the *Aerial Grid or Corridor* flight paths option. For image calibration, extractable keypoints were automatically selected, and the standard methods were used: *Automatic Aerial Triangulation*, *Bundle Block Adjustment*, and camera self-calibration. For point cloud densification, the default image scale (half-size) and point density were used. The resolution of the generated DSM was the same as the resolution of the images. The DSM generation process included noise filtering and surface smoothing. It should be noted that the software cannot edit tie points, probably due to their large number per image pair. The Image Coordinate System was WGS 84 (EGM 96 Geoid), and the Output Coordinate System was ETRS89 / Poland CS2000 zone 5 (EGM 96 Geoid). The basic data related to image processing are summarized in Table 2 (based on the Quality Report generated by Pix4DMapper software).

During processing, based on visual inspection, a large amount of noise was found above-water near the banks and sides of the span, the lighthouses on the bridge, and the radar reflector mounts; therefore, this noise was filtered out manually and removed together with the lighthouse points and the radar reflector mounts due to their shuffling. The noise removal process affected the orthorectification result. Editing involved the local correction of a part of the image, especially the elongation of the span edge where marks and lights were fixed. Figure 5 illustrates the successive steps of orthoimage correction using the example of a streetlamp and radar

Table 2. The basic data related to image processing

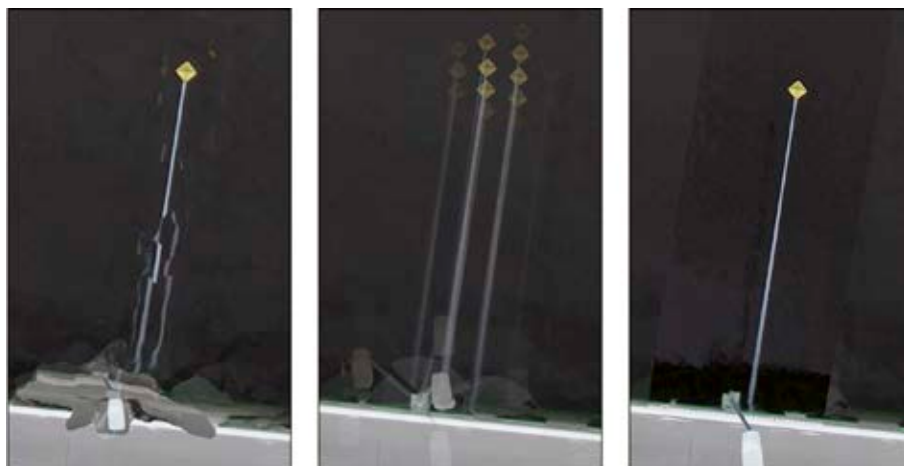|	Dataset 1	Dataset 2	Dataset 3
Percentage of calibrated images	79	84	72
Georeferencing (mean RMS error of 7 GCP) [m]	0.022	0.022	0.023
Number of Matched 2D Keypoints per Image (mean)	6025	4412	2405
Ground Control Points RMS error [m]	X = 0.009, Y = 0.007, Z = 0.052	X= 0.012, Y= 0.008, Z= 0.046	X= 0.009, Y=0.005, Z= 0.058
Area	0.040 km^2	0.035 km^2	0.036 km^2
Photos	396	457	853

Figure 5. Local orthomosaic correction

reflector. The first image, which was created with the system noise reduction option, shows very large distortions of the lamp and the reflector mount. Similar distortions for standing objects were also observed in the work in ref. (Koeva et al., 2018). On the other hand, removing this part of the DSM resulted in their replication in many places, known as the ghost effect (Xue, Zhang & Chen, 2021). These distortions were removed during the manual editing of the orthomosaics. The orthogonal projection options were chosen for the correction, which allows measurements to be made using the final product. Unfortunately, the image fragment in this projection was not always generated correctly; thus, such a process does not entirely allow the preservation of the correct geometry of the photographed objects. Such editing was also necessary when the light was obscured by a streetlamp. This made it necessary to take additional images from land or oblique images from the UAV to ensure that all objects were quantitatively identified to ensure the completeness of the mapped objects.

Image matching

An important step in the development of photogrammetric products is the matching of image feature points, whose number and distribution play an important role in the correctness and accuracy of image matching and orientation results. Mousavi et al. (Mousavi, Varshosaz & Remondino, 2021) indicated that the use of appropriate keypoint selection techniques can improve the entire image block alignment process. Many point extraction algorithms have been developed for various applications (e.g., Wang, Fan & Wu, 2013; Verdie et al., 2015). In the case of photogrammetric software, the extraction

process is often completely automated, without the possibility of correction. This is certainly dictated by the fact that many tie points are often generated (thousands of points per image), which makes manual correction difficult and essentially impractical. For the cases analyzed, the number of matching points for the same area varied. Undoubtedly, this is connected with the flight technique. For the set of photos no. 1, there were on average 6025 matches per photo; for the set of photos no. 3 – 4412; for the last one – 2405. It is certainly worth noting the last case, for which the doubled number of photos did not increase the number of matched keypoints, and even significantly decreased them.

In the implemented processes, a considerable portion of the images was uncalibrated. The highest number of calibrated images was recorded for flight 2 (84%), followed by flight 3 with 79%, and the lowest for the combined set with 72%. Analyzing the location of uncalibrated images, we can conclude that these are images were taken over water due to the lack of a possibility to generate characteristic points, which was connected with the uniform structure of water and also its variability caused by the river current. Due to the lack of use of these parts of the water body in mapping, their absence from the final product is not a major problem, except perhaps for the completeness of the image and aesthetic aspects. It should also be noted that despite the high mutual overlap of the images (90%), a uniform block of images was not obtained for flight 1. This block was divided into two parts, which undoubtedly affected the accuracy of the final study.

In addition, the software could be used to analyze the quality of the matching based on uncertainty ellipses (Figure 6), which tend to be larger at the edges of the image block and smallest in the middle.
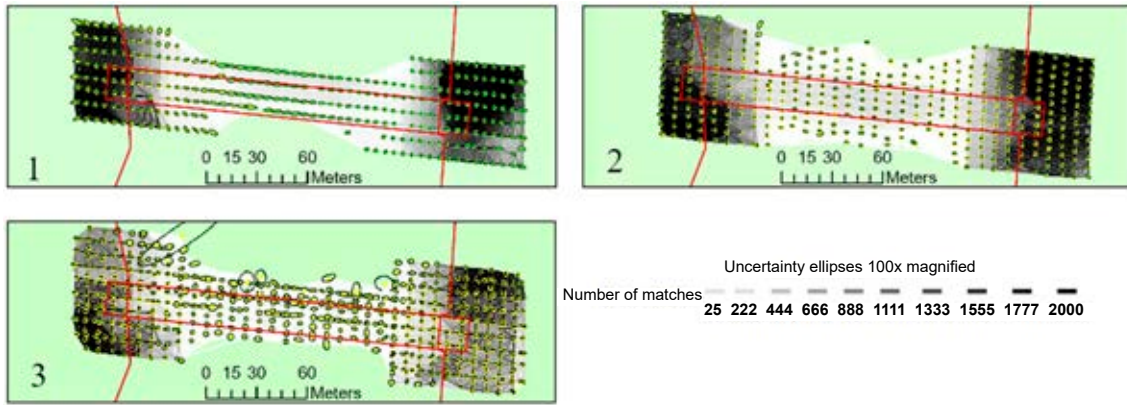
Figure 6. Match distribution and uncertainty ellipses for image sets 1, 2, and 3

As can be seen, such a relationship occurred in the second set of images. The uncertainty ellipses for the first set of images were larger on the bridge span due to the processing of the data as two separate blocks of images. In the case of the third set of photos, their shapes were irregular, including the occurrence of large uncertainty ellipses, which indicates problems with the merging of the photos in the whole block. Some of the uncertainty ellipses were located in the centers of the projection of the photos over water. Nevertheless, the ellipses have different sizes on the bridge span, indicating problems with matching them. In addition, the merged set of photos eliminated the problem that occurred with photo set 1.

Another element of the analysis is the number of image matches. The minimum number of matches is 25, while the optimum is more than 1000. Analyzing the maps of matches shows that in all cases, the number of matches decreased significantly at the span of the bridge. Both cases are illustrated in Figure 6. For image sets 1 and 3, the number of matches was very small – about 25. The best case was image set 2, where the number of matches ranged from 25 to 222.

In the cases analyzed, the location of the tie points is also interesting. The fewest points were located on the asphalt roadway. A greater number of them were observed on horizontal markings, which is certainly an advantage for this type of facility. A much larger number of tying points were located on pedestrian walkways, road safety barriers, and fewer on the railings. The highest number of tie points was in the land area of the study, which has a varied structure, causing many tie points to be generated. A view of the generated tie points is illustrated in Figure 7.

Results

Qualitative analysis

The final orthophoto product was highly detailed and of good quality. Marks and lights could be identified from the image, along with the measurement points (Figure 8a). It was also noticed that the span edge was not very well represented – in some places, it was not clearly marked and had slight artefacts (Figure 8b). Additionally, after local correction of the orthophoto fragments, the effect of patches was noticed, which affected the aesthetics of the final work (Figure 8c). In some cases, it was not possible to select a suitable orthophoto for local correction, so hence the object was not reproduced correctly in its entirety (Figure 8d). The continuous lines of the horizontal markings were mapped correctly, which also demonstrates the correctness of the orthomosaic generation. Undoubtedly, the final product meets the technical requirements in terms of the identification
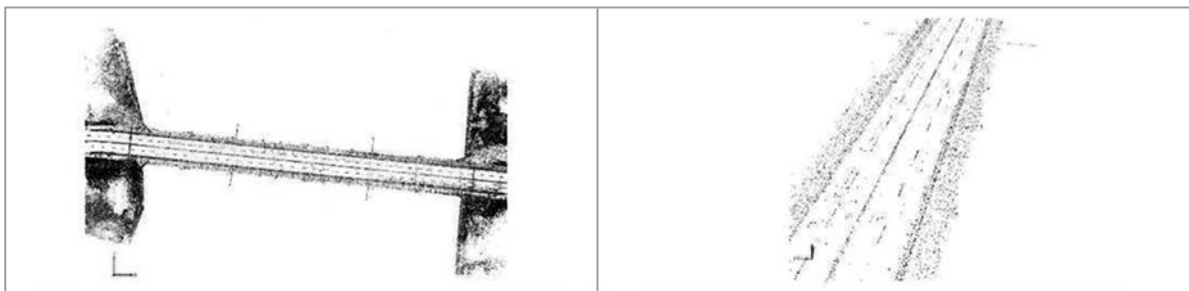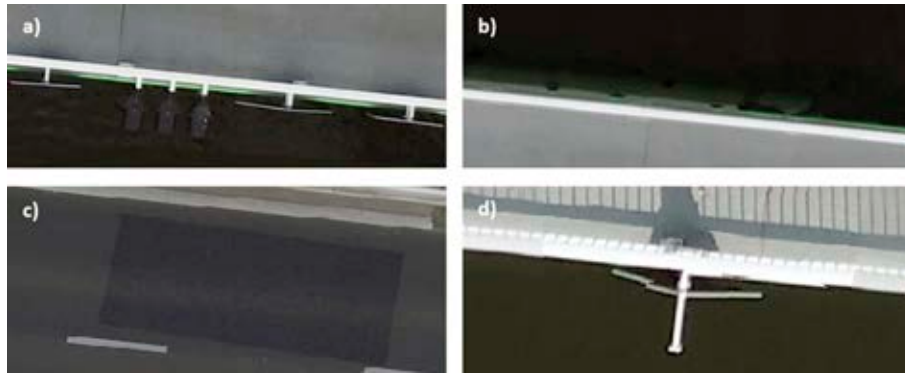

Figure 7. The view of tie points

Figure 8. Analyzed cases of qualitative assessment: a) lights and marks, b) edge of the bridge span, c) effect of car removal, and d) uncorrected object with a broken sign effect

of surveyed objects and the acquisition of vector data with centimeter accuracy.

Quantitative analysis

The quantitative assessment was carried out based on:

(1) Mean deviations (r_m) of points acquired from orthoimage (x_o, y_o) and points (x_g, y_g) measured with a GNSS RTK receiver. Additionally, the minimum and maximum values of the obtained deviations were analyzed. Calculations were performed separately for 10 marks ($k = 10$) and 18 lights ($k = 18$). In the case of the bridge span, the deviations were measured on the section orthogonal to the vectorized bridge segment at 13 points ($k = 13$). The mean deviations were calculated according to the following formula:

$$r_m = \frac{\sum_{i=1}^{k}\sqrt{\left(x_{o_i} - x_{g_i}\right)^2 - \left(y_{o_i} - y_{g_i}\right)^2}}{k} \qquad (1)$$

(2) Mean difference in the distance between consecutive marks and lights located on two sides of the span ($k = 12$ for each span). Additionally, the minimum and maximum values were analyzed. The calculation of the difference involved subtracting the distance between them in the orthophoto (d_{oi}) from the distance calculated based on RTK (d_{gi}) measurements. The aim of this analysis was to determine the relative accuracy, i.e., if the mapped marks and lights showed similar distances to the real values (they were not unnaturally distant from each other or close). The mean differences (d_m) were calculated using the following formula:

$$d_m = \frac{\sum_{i=1}^{k}\left|d_{o_i} - d_{g_i}\right|}{k} \qquad (2)$$

Tables 3 and 4 summarize the values analyzed.

Table 3. Analyzed values of deviations

Objects	Image dataset	r_m [m]	$r_{\min}$ [m]	$r_{\max}$ [m]
Navigational marks	Dataset 1	0.14	0.07	0.29
	Dataset 2	0.05	0.02	0.09
	Dataset 3	0.05	0.01	0.12
Lights	Dataset 1	0.08	0.01	0.22
	Dataset 2	0.04	0.02	0.08
	Dataset 3	0.03	0.01	0.05
Bridge span	Dataset 1	0.06	0.01	0.10
	Dataset 2	0.06	0.01	0.11
	Dataset 3	0.06	0.03	0.10

Table 4. Analyzed values of relative accuracies

Span side	Dataset	r_m [m]	$d_{\min}$ [m]	$d_{\max}$ [m]
Northern	Dataset 1	0.05	0.01	0.26
	Dataset 2	0.01	0.00	0.08
	Dataset 3	0.02	0.00	0.07
Southern	Dataset 1	0.03	0.00	0.09
	Dataset 2	0.01	0.00	0.04
	Dataset 3	0.02	0.00	0.08

Based on the results in Table 3, it can be concluded that the best results were obtained for datasets 2 and 3. The mean errors had values up to 6 cm and maximum errors up to 12 cm. Dataset 1 showed the highest maximum error of 29 cm. In terms of relative accuracy (Table 4), the highest value of the mean error was 5 cm in all cases. The highest maximum errors were recorded for measurement set 1. Analyzing the magnitude of the errors along the bridge span, it can be concluded that they do not show much dependence on the number of tie points or specific parts of the bridge. Some regularity was noted in case no. 1 (Figure 9), where larger errors occurred in the middle part of the span. For the second set of measurements, larger errors occurred on

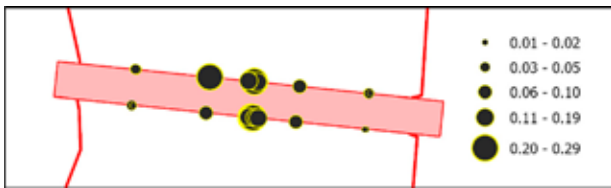the right side of the span (Figure 10), and for set no. 3, their magnitude varied (Figure 11).

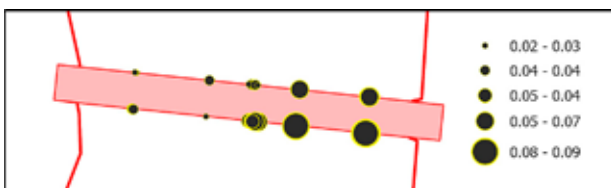**Figure 9. Signature map of deviations (cm) from marks and lights for set no. 1**

Figure 10. Signature map of deviations (cm) from marks and lights for set no. 2
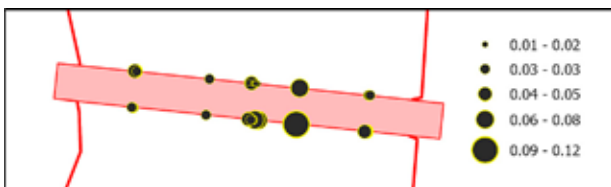

Figure 11. Signature map of deviations (cm) from marks and lights for set no. 3

Figure 12 shows a map with vectorized marks, lights, and bridge span as elements of an electronic navigational chart for inland navigation.

Figure 12. Mapped marks, lights, and span on the IENC map

Conclusions

Based on the conducted research, it can be concluded that the use of low-altitude photogrammetric data allows for the mapping of marks, lights, and bridge spans within the required accuracy. The obtained accuracies significantly exceed the requirements related to the development of IENC

maps (1 m). Due to the higher accuracies obtained and the better matching of the photos during the ortho generation process, the camera sensor should be positioned with its longer side along the bridge axis during measurements. Increasing the number of images by longitudinal and transverse flights over the bridge produced similar accuracies, so a single mission is sufficient. This certainly shortens the mission time and increases the safety of the entire operation. The high relative accuracy between marks and lights guarantees their correct positioning on the map along the span of the bridge. In the case of the bridge, the orthophoto study required manual corrections of mosaicking. It was also found that the edges of the bridge span were not reproduced very accurately, which slightly deteriorated the photo-interpretation properties of the final product; therefore, additional oblique photographs will be helpful for photo-interpretation. After applying manual mosaicking corrections, a poor tonal alignment of the image was obtained. During the development of photogrammetric products of bridges, attention should be paid to the type of pavement and the various structures on it (road safety barriers and railings), as these can significantly impact the generation of tie points and subsequently the alignment accuracy of the image block.

Acknowledgments

References

1. Angnuureng, D.B, Jayson-Quashigah, P.-N, Almar, R, Stieglitz, T.C, Anthony, E.J, Aheto, D.W & Addo, K.A. (2020) Application of Shore-based Video and Unmanned Aerial Vehicles (Drones): Complementary Tools for Beach Studies. *Remote Sensing* 12(3), 394, doi: 10.3390/rs12030394.

2. Casella, E., Drechsel, J., Winter, C., Benninghoff, M. & Rovere, A. (2020) Accuracy of Sand Beach Topography Surveying by Drones and Photogrammetry. *Geo-Marine Letters* 40, pp. 255–268, doi: 10.1007/s00367-020-00638-8.

3. Contreras-De-Villar, F., García, F.J., Muñoz-Perez, J.J., Contreras-De-Villar, A., Ruiz-Ortiz, V., Lopez, P., Garcia-López, S. & Jigena, B. (2021) Beach Leveling Using a Remotely Piloted Aircraft System (RPAS): Problems and Solutions. *Journal of Marine Science and Engineering* 9(1), 19, doi: 10.3390/jmse9010019.

4. Burdziakowski, P. (2021) Polymodal Method of Improving the Quality of Photogrammetric Images and Models. *Energies* 14(12), 3457, doi: 10.3390/en14123457.

5. Burdziakowski, P., Specht, C., Dabrowski, P.S., Specht, M., Lewicka, O. & Makar, A. (2020) Using UAV Photogrammetry to Analyse Changes in the Coastal Zone Based on the Sopot Tombolo (Salient) Measurement Project. *Sensors* 20(14), 4000, doi: 10.3390/s20144000.

6. Chen, W.F. & Duan, L. (Eds.) (2003) *Bridge Engineering: Substructure Design. 1st Edition.* CRC Press, doi: 10.1201/9780203009079.

7. Escobar-Wolf, R., Oommen, T., Brooks, C.N., Dobson, R.J. & Ahlborn, T.M. (2018) Unmanned Aerial Vehicle (UAV)-Based Assessment of Concrete Bridge Deck Delamination Using Thermal and Visible Camera Sensors: A Preliminary Analysis. *Research in Nondestructive Evaluation* 29, 4, pp. 183–198, doi: 10.1080/09349847.2017.1304597.

8. Ikeda, T., Yasui, S., Minamiyama, S., Ohara, K., Ashizawa, S., Ichikawa, A., Okino, A., Oomichi, T. & Fukuda, T. (2018) Stable impact and contact force control by UAV for inspection of floor slab of bridge. *Advanced Robotics* 32(19), pp. 1061–1076, doi: 10.1080/01691864.2018.1525075.

9. Jung, S., Song, S., Kim, S., Park, J., Her, J., Roh, K. & Myung, H. (2019) *Toward Autonomous Bridge Inspection: A framework and experimental results*. 16th International Conference on Ubiquitous Robots (UR), pp. 208–211, doi: 10.1109/URAI.2019.8768677.

10. Kedzierski, M., Wierzbicki, D., Sekrecka, A., Fryskowska, A., Walczykowski, P. & Siewert, J. (2019) Influence of Lower Atmosphere on the Radiometric Quality of Unmanned Aerial Vehicle Imagery. *Remote Sensing* 11(10), 1214, doi: 10.3390/rs11101214.

11. Khaloo, A., Lattanzi, D., Cunningham, K., Dell'andrea, R. & Riley, M. (2018) Unmanned aerial vehicle inspection of the Placer River Trail Bridge through image-based 3D modelling, *Structure and Infrastructure Engineering* 14(1), pp. 124–136, doi: 10.1080/15732479.2017.1330891.

12. Kim, I.-H., Jeon, H., Baek, S.-C., Hong, W.-H. & Jung, H.-J. (2018) Application of Crack Identification Techniques for an Aging Concrete Bridge Inspection Using an Unmanned Aerial Vehicle. *Sensors* 18(6), 1881, doi: 10.3390/s18061881.

13. Knott, M. & Winters, M. (2018) *Ship and barge collisions with bridges over navigable waterways*. PIANC – World Congress, Panama City, Panama.

14. Koeva, M., Muneza, J.M., Gevaert, C., Gerke, M. & Nex, F. (2018) Using UAVs for map creation and updating. A case study in Rwanda. *Survey Review* 50(361), pp. 312–325, doi: 10.1080/00396265.2016.1268756.

15. Kujawski, A., Jerzyło, P. & Rekowska, P. (2018) Shipping Safety Management on Polish Inland Waterways. *Archives of Transport System Telematics* 11, 4, pp. 18–22.

16. Lizarazo, I., Angulo Morales, V. & Rodríguez Galvis, J. (2017) Automatic mapping of land surface elevation changes from UAV-based imagery. *International Journal of Remote Sensing* 38(1), pp. 2603–2622, doi: 10.1080/01431161.2016.1278313.

17. Lopatin, E. & Lopatina, A. (2017) Assessing and mapping energy biomass distribution using a UAV in Finland. *Biofuels* 8(4), pp. 485–499, doi: 10.1080/17597269.2017.1302663.

18. Lowe, M.K., Adnan, F.A.F., Hamylton, S.M., Carvalho, R.C. & Woodroffe, C.D. (2019) Assessing Reef-island Shoreline Change Using UAV-derived Orthomosaics and Digital Surface Models. *Drones* 3(2), 44, doi: 10.3390/drones3020044.

19. Łubczonek, J., Łącka, M. & Zaniewicz, G. (2019) Analysis of the accuracy of shoreline mapping in inland navigational charts (Inland ENC) using photogrammetric and sonar images. *Scientific Journals of the Maritime University of Szczecin, Zeszyty Naukowe Akademii Morskiej w Szczecinie* 58(130), pp. 45–54, http://dx.doi.org/10.17402/335.

20. Łubczonek, J. (2017) The use of terrestrial laser scanning for mapping bridges on electronic navigational charts. *Annals of Geomatics* XV, 2(77), pp. 217–232.

21. Mac, V.H., Tran, Q.H., Huh, J., Doan, N.S., Kang, C. & Han, D. (2019) Detection of Delamination with Various Width-to-depth Ratios in Concrete Bridge Deck Using Passive IRT: Limits and Applicability. *Materials* (Basel, Switzerland) 12(23), 3996, doi: 10.3390/ma12233996.

22. Mousavi, V., Varshosaz, M. & Remondino, F. (2021) Using Information Content to Select Keypoints for UAV Image Matching. *Remote Sensing* 13(7), 1302, doi: 10.3390/s18061881.

23. Tsukada, F., Shimozono, T. & Matsuba, Y. (2020) UAV-based mapping of nearshore bathymetry over broad areas. *Coastal Engineering Journal* 62, 2, pp. 285–298, doi: 10.1080/21664250.2020.1747766.

24. Verdie, Y., Yi, K.M., Fua, P. & Lepetit, V. (2015) *TILDE: A Temporally Invariant Learned DEtector*. In Proceedings of the IEEE Conference on Computer Vision and Pattern Recognition, Boston.

25. Wang, Z., Fan, B. & Wu, F. (2013) *FRIF: Fast Robust Invariant Feature*. In Proceedings of the BMVC, Bristol, UK.

26. Xue, W., Zhang, Z. & Chen, S. (2021) Ghost Elimination via Multi-Component Collaboration for Unmanned Aerial Vehicle Remote Sensing Image Stitching. *Remote Sensing*, doi: 10.3390/rs13071388.